Shock Waves (2005) 14(5/6): 371–378
DOI 10.1007/s00193-005-0276-3

ORIGINAL ARTICLE

R. R. Boyce · M. Takahashi · R. J. Stalker

Mass spectrometric measurements of driver gas arrival in the T4 free-piston shock-tunnel

Received: 24 April 2003 / Accepted: 11 August 2005 / Published online: 27 October 2005

Abstract Available test time is an important issue for ground-based flow research, particularly for impulse facilities such as shock tunnels, where test times of the order of several ms are typical. The early contamination of the test flow by the driver gas in such tunnels restricts the test time. This paper reports measurements of the driver gas arrival time in the test section of the T4 free-piston shock-tunnel over the total enthalpy range 3–17 MJ/kg, using a time-of-flight mass spectrometer. The results confirm measurements made by previous investigators using a choked duct driver gas detector at these conditions, and extend the range of previous mass spectrometer measurements to that of 3–20 MJ/kg. Comparisons of the contamination behaviour of various piston-driven reflected shock tunnels are also made.

Keywords Time-of-flight mass spectrometer · Shock tunnel · Driver gas contamination · Test time

PACS 07.75.th; 47.40.-x

1 Introduction

Aerodynamic or propulsion system research in impulse facilities such as the hypervelocity free-piston shock-tunnel [1] is constrained by the length of available test time. This is particularly important for the full development of steady flow on a given test model, where, for example, boundary layer separation and large subsonic pockets may be important. For a given flow speed, the length of test gas slug required for steady establishment dictates a minimum test time required.

Shock tunnels operate by heating and compressing a slug of test gas with a reflected shock in a shock tube. This processed gas then expands through a hypersonic nozzle into the test section. The drainage of test gas from the shock tube into the nozzle provides the ultimate limitation on available test time. For example, the ideal maximum flow duration for the T4 shock tunnel at The University of Queensland, at a total enthalpy of 10 MJ/kg (equivalent to a flight speed of 4.5 km/s) is approximately 5 ms [2]. The degree of driver/test gas interface tailoring obtained in the operation of the tunnel influences the driver gas arrival time. With tailored interface operation, the driver/test gas contact surface is brought to rest by the reflected shock. With overtailored operation, the contact surface retains some velocity towards the nozzle and the arrival of the driver gas in the test section thus occurs earlier.

However, it is well established [3, 4] that significant loss of test time occurs in reality due to early arrival of the driver gas at the entrance to the nozzle. The most important mechanism for this is bifurcation of the reflected shock in the shock tube, associated with separation of the shock tube wall boundary layer that developed behind the primary shock. Jetting of boundary layer gas through the bifurcation towards the nozzle occurs. When the bifurcated shock reaches the contact surface between the test gas and the driver gas (usually a mixture of helium and argon), driver gas jetting occurs, resulting in early contamination of the test gas. Experimental measurements of test gas contamination in the T2 and T3 shock tunnels at the Australian National University [5] and the T5 shock tunnel at CalTech [6] have shown reasonable agreement with predictions using the bifurcation model of Davies and Wilson [3]. Furthermore, overtailored interface operation was observed to result in much earlier contamination than for tailored operation

Communicated by K. Takayama

R. R. Boyce (✉)
Formerly Mechanical Engineering, University of Queensland, Australia
School of Aerospace, Civil and Mechanical Engineering, University College, University of New South Wales, Australian Defence Force Academy, Canberra 2600, Australia
E-mail: r.boyce@adfa.edu.au

M. Takahashi
Japanese Aerospace Exploration Agency, Kakuda Space Center, 1 Koganesawa, Kimigaya, Kakuda-shi, Miyagi 981-1525, Japan

R. J. Stalker
Division of Mechanical Engineering, University of Queensland, Brisbane 4072, Australia

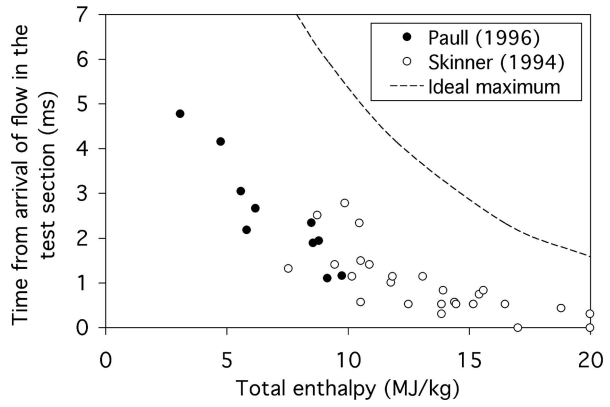

Fig. 1 Previous measurements in T4 of available test time prior to 7.5% [7] and 10% [2] driver gas contamination, and the ideal maximum time based on drainage

[6]. More recently, computational fluid dynamics (CFD) simulations of reflected shock tunnels have been made (for example, Chue and Eitelberg [8], Burtschell et al. [9], Goozee [10]) that capture this phenomenon. In particular, Goozee [10] shows that vortices generated by the bifurcated shock structure interact with the driver gas and carry some of it towards the centre of the shock tube and into the nozzle.

Measurements of driver gas contamination in T4 have been made by Skinner [2] over the total enthalpy range 8–20 MJ/kg using a time-of-flight mass spectrometer, and also by Paull [7] over the total enthalpy range 3–9.5 MJ/kg, using a choked duct device. Both sets of results are summarised in Fig. 1, which shows the measured time (after the first arrival of flow in the test section) taken for driver gas contamination of the flow to reach 7.5% (in the case of [7]) and 10% (in the case of [2]). Also shown on the figure is the approximate ideal test time according to Skinner [2]. Clearly, driver gas contamination presents a serious degradation of available test time, reducing it by approximately 3–4 ms. This limits the useful maximum total enthalpy of the tunnel to values of the order of 12 MJ/kg. While this poses issues for re-entry flowfield research, significant test time is still available for scramjet flows. For example, for scramjet tests at flight Mach number 10, the required total enthalpy is approximately 5 MJ/kg. The data presented in Fig. 1 suggests that at least 2 ms of test time would be available in T4 for such a case.

However, the signal-to-noise ratio obtained by Skinner [2] was at times poor, while the experiments of Paull [7] were restricted to low enthalpy flows to avoid the complicating influence of real gas effects on the results. The two sets of data do not overlap sufficiently to confirm each other.

Accordingly, successful efforts have been made to improve the signal-to-noise ratio of the mass spectrometer, and further shock tunnel experiments have been conducted. This paper presents extensive experimental results for the arrival time of the driver gas in the test section of the T4 free-piston shock-tunnel, for total enthalpies in the range 3–17 MJ/kg. This range covers that of both Paull [7] and Skinner [2].

Table 1 Operating conditions

	Low enthalpy	High enthalpy
v_s	1.52 ± 0.08 km/s	4.07 ± 0.20 km/s
P_o	20.5 ± 0.6 MPa	36.0 ± 1.1 MPa
T_o	2126 ± 130 K	8221 ± 490 K
h_o	2.44 ± 0.15 MJ/kg	16.9 ± 1.0 MJ/kg
He	0%	85%
Ar	100%	15%

2 The experiment

The results reported here were obtained from experiments in the T4 free-piston reflected shock tunnel. The stagnation enthalpy was varied from 3 to 17 MJ/kg (by adjusting the shock tube initial pressure and hence the primary shock speed), and the nozzle supply pressure was varied from 12 to 40 MPa (by varying the tunnel primary diaphragm thickness from 2 to 5 mm mild steel). An extensive series of experiments were performed in which the centre-line freestream composition produced by a nominal Mach 6 contoured nozzle was measured with the time-of-flight mass spectrometer. During the same experiments, the time resolved mass spectra enabled both the relative composition of the test gas (reported by Boyce et al. [11]) and the eventual arrival of the driver gas to be investigated. A detailed description of the design and operation of the mass spectrometer is provided by Boyce et al. [11], and will not be repeated here.

Eighteen different operating conditions with air as the test gas were utilised in the present work, spread over the range of stagnation pressures and enthalpies attained. In addition, 30 different operating conditions for the four calibration mixture test gases were used. Table 1 presents the nozzle supply conditions for the air runs, determined as described by Boyce et al. [11] for the two enthalpy extremes. The driver gas composition is also specified in the table. In all of the experiments, effort was made to avoid overtailored interface operation. Thus, each operating condition is tailored or undertailored, the latter accompanied by at worst a 10% decay in nozzle reservoir pressure per millisecond during the period prior to 10% contamination levels for each condition.

3 Data analysis

The mass spectrometer provides complete mass spectra of the species of interest in the tunnel every 53 μs, thus giving more than 100 spectra during the recorded 6 ms of flow time. By averaging adjacent groups of five spectra, the quality of the mass peaks is improved, but at the expense of temporal resolution, with composition results determined every 265 μs. Figure 2 provides an example of an averaged mass spectrum for a $h_o = 8.2$ MJ/kg run. The identity of the peaks in the figure are labelled. Note the presence of He and Ar at this time in the flow.

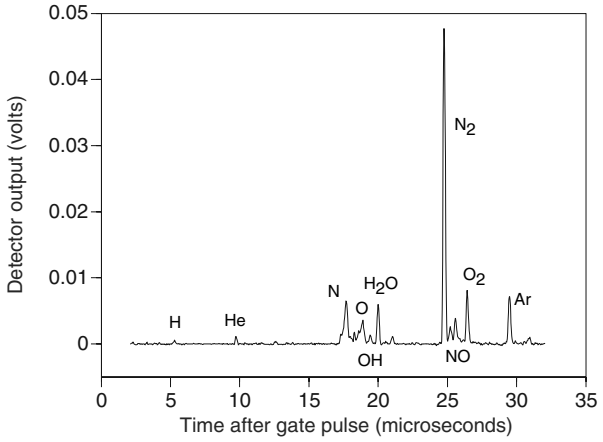

Fig. 2 Typical averaged spectrum 4.11 ms after primary shock arrival at nozzle entrance (8.2 MJ/kg)

The details of the analysis of the mass spectra is given by Boyce et al. [11], and will not be repeated here.

Typical mass spectra peak area time histories are presented in Figs. 3 and 4. These figures show the peak areas for N_2, He and Ar, normalised by the sum of N_2, O_2, NO, N, O, He and Ar, for low (3.0 MJ/kg) and moderately high (10.7 MJ/kg) total enthalpies, respectively. The fluctuations evident in the time histories are due partly to fluctuations in the relative levels of test and driver gases in the sampled gas, and partly to the experimental uncertainty associated with the resolution (detection and analysis) of small mass spectra peaks. As will be discussed later, the extent of the resolution uncertainty is determined to be approximately ± 0.01 (absolute) for any peak area ratio with the N_2 peak. Sample error bars accounting for this uncertainty are shown on the figures. In Figs. 3 and 4, the increase with time in the levels of the driver gas components present in the freestream flow is evident, and is clearly of much more significance at higher total enthalpy. Note that in Fig. 4 the Ar peak areas are much greater than the He peak areas, despite the driver gas being predominantly He in that case. This is a reflection of the ease of ionisation of Ar relative to He in the mass spectrometer.

As described in detail by Boyce [11], the processes of sampling the flow, ionising the species, accelerating/deflecting them into a drift tube for mass separation, and finally detecting the ions alter the relative composition of the gas. To convert relative peak areas (which correspond to relative species concentrations recorded by the detector) to values for the freestream composition, calibration factors have been determined using tunnel runs with non-reactive calibration mixtures and very low enthalpy air runs (for which no freestream dissociation is expected). The calibration mixtures include mixtures of N_2 and He and mixtures of N_2 and Ar. The details of the calibration process are provided by Boyce et al. [11], in which it is shown that to within experimental uncertainty there was no dependence on flow total enthalpy of the relative mass spectra peak areas for N_2, He and Ar. This conclusion is important for the work presented here.

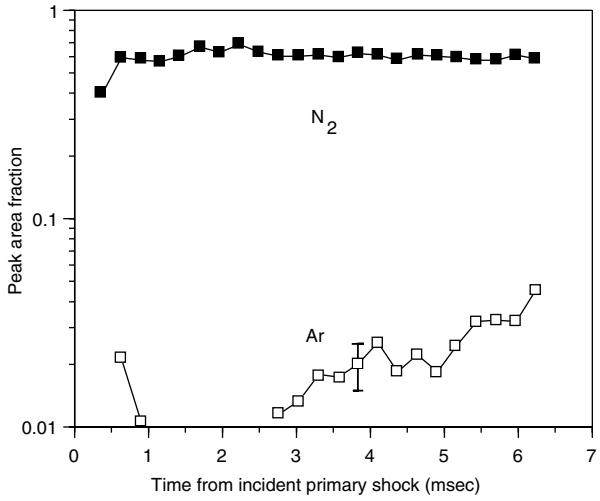

Fig. 3 Typical normalised peak area time histories for $h_o = 3.0$ MJ/kg (driver gas: 100% Ar)

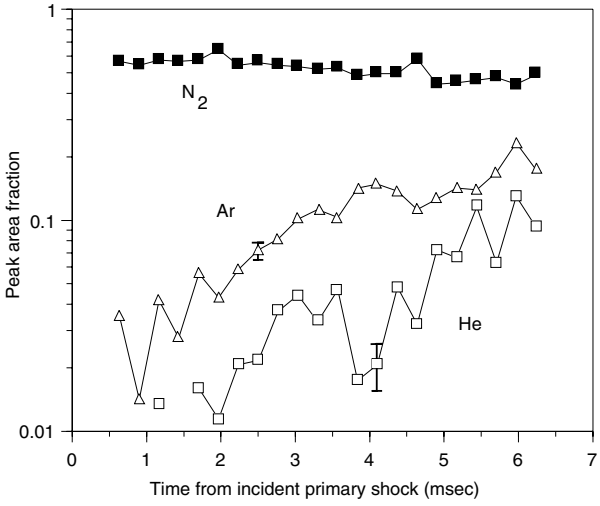

Fig. 4 Typical normalised peak area time histories for $h_o = 10.7$ MJ/kg (driver gas: 20% Ar; 80% He)

The following calibration factors are yielded for each species X relating the measured peak area A_X (normalised by the N_2 peak area) to the freestream mole fraction x_X (normalised by the N_2 mole fraction). These calibration factors are given in Eq. (1) for N_2, He and Ar (see [11] for the other components of air). The uncertainties account for the standard deviations in the averaged peak area ratios determined from the calibration shots, and also include the published uncertainties for the ionisation cross-sections.

$$\bar{A} = \mathbf{C}\bar{x} \tag{1}$$

where $\bar{A}^T = \left(\frac{A_{N_2}}{A_{N_2}} \; \frac{A_{He}}{A_{N_2}} \; \frac{A_{Ar}}{A_{N_2}} \right)$, $\bar{x}^T = \left(\frac{x_{N_2}}{x_{N_2}} \; \frac{x_{He}}{x_{N_2}} \; \frac{x_{Ar}}{x_{N_2}} \right)$ and

$$\mathbf{C} = \begin{pmatrix} 1 & 0 & 0 \\ 0 & 0.071 \pm .015 & 0 \\ 0 & 0 & 0.96 \pm .12 \end{pmatrix}$$

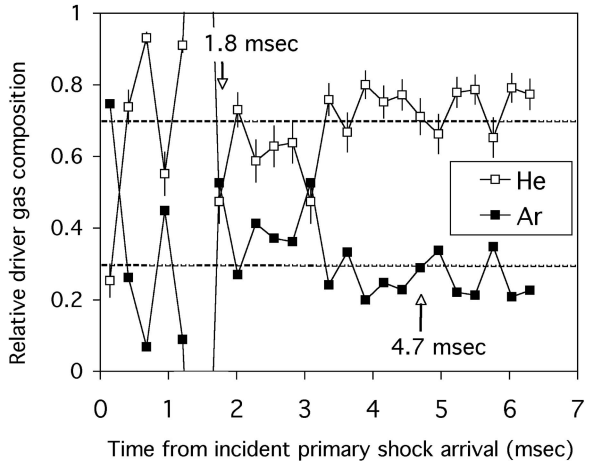

Fig. 5 Time history of the measured relative composition of He and Ar for 7.6 MJ/kg (driver gas: 30% Ar; 70% He)

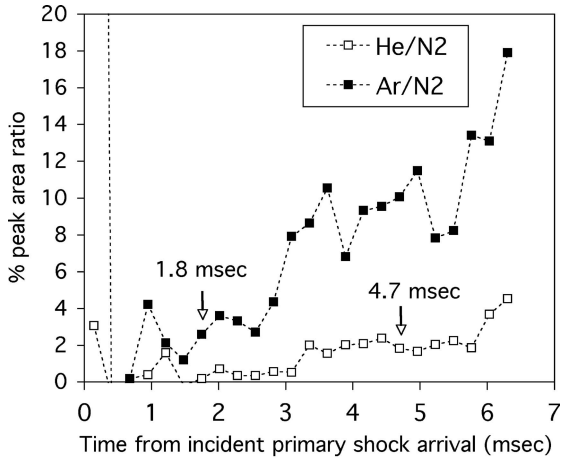

Fig. 6 Time history of the peak area ratios (%) for He/N_2 and Ar/N_2 for 7.6 MJ/kg (driver gas: 30% Ar; 70% He)

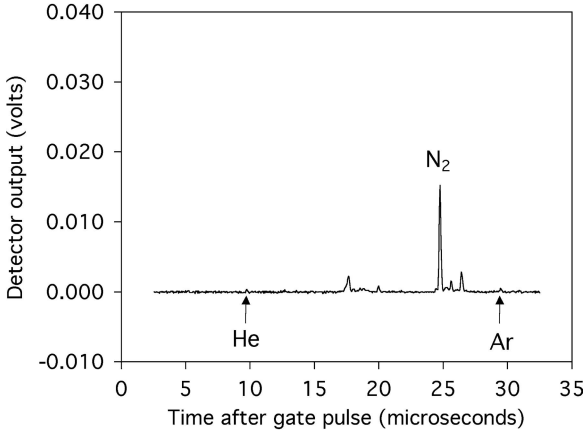

Fig. 7 Averaged spectrum 1.8 ms after primary shock arrival at nozzle entrance (7.6 MJ/kg)

.

It should be noted that the calibration factors were obtained from mixtures in which the minor component (such as He or Ar) still represented a reasonable fraction of the mixture, typically 20% or more. Since the purpose of the present work is to investigate the arrival of such species in the test gas, an estimate of the errors associated with the resolution of small mass spectral peaks is necessary. This can be done by extracting from the experimental data the ratio of He and Ar as a function of time throughout each run—this should ideally remain fixed and conform to the known ratio initially used for the driver gas, but is determined from comparing spectral peaks which grow from initially zero size throughout the duration of each run.

By manipulating Eq. (1), the driver gas relative mole fractions are given by

$$\frac{x_{\mathrm{Ar}}}{x_{\mathrm{He}}} = 0.074 \frac{A_{\mathrm{Ar}}}{A_{\mathrm{He}}} \tag{2}$$

Employing Eq. (2), Fig. 5 presents the time history of the relative proportions of Ar and He measured in the test section for a shot with total enthalpy 7.6 MJ/kg. The original driver gas proportions were 30% Ar and 70% He. The results show that after the first 3 ms of flow the measured relative concentrations agree with the expected proportions. Prior to this time, the peaks are too small to obtain sensible measurements. Inspection of the complete set of data yields the conclusion that sensible driver gas ratios are obtained when the He peak area is at least 2% of the N_2 peak area. This is demonstrated in Fig. 6, which shows the peak area ratios for Ar/N_2 and He/N_2 expressed as percentages for the run of Fig. 5. It is further demonstrated in Figs. 7 and 8, which show the averaged mass spectra for that run at 1.8 and 4.7 ms after primary shock reflection, respectively. In the first spectrum, the Ar peak is approximately 3% of the N_2 peak, and because He atoms are ionised by electron impact much less efficiently than Ar atoms, the He peak is extremely small. Driver gas ratios obtained from this spectrum are very inaccurate. On the other hand, the He and Ar peaks in the second spectrum are large enough to yield sensible ratios. A further example for a 12.0 MJ/kg, 20% Ar, 80% He run is given in Fig. 9. The driver gas levels are higher at earlier times in this case, and sensible driver gas ratios are observed after approximately 1 ms. The conclusion to be drawn here is that the resolution of this instrument is limited to peaks that are of the order of 2% of the large N_2 peak area.

The error bars on the He data in Figs. 5 and 9 combine the uncertainties in the calibration factors for He and Ar. They have been applied to the He data only, because the Ar data in those figures are actually just the He results subtracted from unity. The calibration factor uncertainties account mainly for run to run fluctuations for mixtures where the minor peaks are much greater in size than the resolution limits of the instrument. In Figs. 5 and 9, it is seen that the driver gas levels fluctuate around their nominal values to a larger extent than the calibration factor uncertainties. Furthermore, this fluctuation is greater in Fig. 5 where the He peak areas remain near the resolution limit. This indicates an

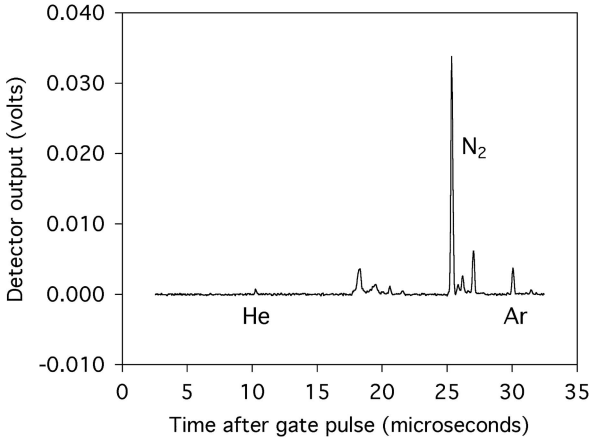

Fig. 8 Averaged spectrum 4.7 ms after primary shock arrival at nozzle entrance (7.6 MJ/kg)

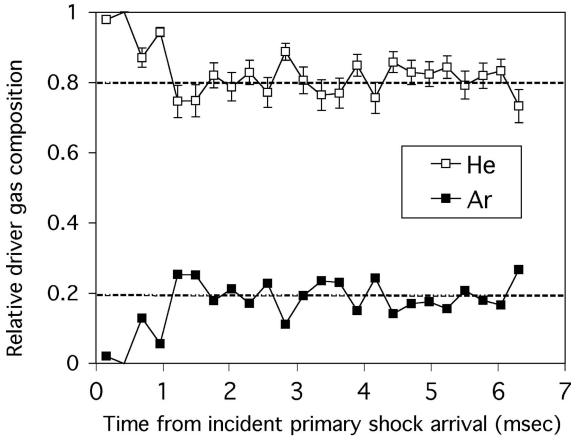

Fig. 9 Time history of the measured relative composition of He and Ar for 12.0 MJ/kg (driver gas: 20% Ar; 80% He)

uncertainty in relative driver gas fractions due to the spectral peak measurement resolution of the instrument of the order of ± 0.1, and can be used in an error analysis employing Eq. (2) to estimate the resolution uncertainty in peak area ratios. This is determined to be approximately ± 0.01 (absolute) for the resolution uncertainty for any peak area ratio with the N_2 peak. Thus, for Fig. 6, the uncertainties (not displayed) for the data shown would be represented by error bars of size ± 1.

For the remainder of this paper, the following assumption is made to avoid inaccuracies in the driver gas measurements in the early stages of each shot due to small He peaks—that by using the Ar measurements only, combined with the knowledge of the original driver gas proportions, the overall driver gas levels in the test section can be inferred. To do this, we assume that the freestream contains only N_2, O_2, NO, He and Ar, since as shown [11], no N or O is detected by the instrument other than that produced by dissociative ionisation inside the instrument itself. Using calibration factors reported here for He and Ar and in [11] for N_2, O_2 and NO, and

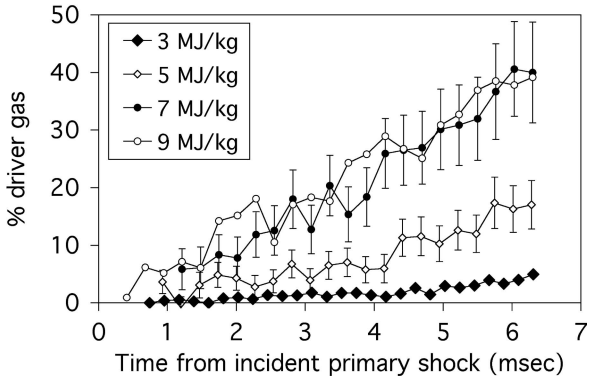

Fig. 10 Time history of driver gas % for various total enthalpies

writing the percentage of Ar originally in the driver as

$$y_{\mathrm{Ar}} = \frac{x_{\mathrm{Ar}}}{x_{\mathrm{He}} + x_{\mathrm{Ar}}} \tag{3}$$

we can deduce the following equation for the % of driver gas in the freestream

$$\%_{\mathrm{d.g.}} = \frac{1.042\frac{A_{\mathrm{Ar}}}{y_{\mathrm{Ar}}}}{1.042\frac{A_{\mathrm{Ar}}}{y_{\mathrm{Ar}}} + 0.877A_{\mathrm{NO}} + 1.053A_{\mathrm{O_2}} + A_{\mathrm{N_2}}} \tag{4}$$

4 Results

Examples of the time histories of the freestream driver gas levels for four enthalpies (approximately 3, 5, 7 and 9 MJ/kg) are given in Fig. 10, and show that the level of driver gas increases approximately linearly as time progresses in each tunnel run (this is observed to occur in the majority of cases, but not all), and also that there is a rapid increase in driver gas levels with increasing total enthalpy. The error bars shown for the 5 and 7 MJ/kg cases account for the uncertainties in the calibration factors and the peak resolution uncertainty. The time history for each case fluctuates to an extent that is of the order of these uncertainties. However, the calibration factor uncertainties represent a systematic component which should be removed in order to assess the extent of the fluctuations. If this is done, then the effect on (for example) the 7 MJ/kg distribution shown in the figure is to decrease the error bar sizes by approximately 10% for the lowest driver gas level and more than 50% at the highest level. The same is true for the 9 MJ/kg level, and the resulting conclusion is that the contamination of the freestream is not smoothly increasing, but rather possesses a degree of turbulent behaviour.

Figure 11 presents the variation with total enthalpy of the driver gas arrival time in the test section, relative to the first arrival of flow in the test section, for three levels of contamination: 5, 10 and 30%, respectively. These results have been extracted from the data by fitting curves to it in order to reduce the scatter that would result if the actual data (with its temporal fluctuations) were used. In this way an estimate

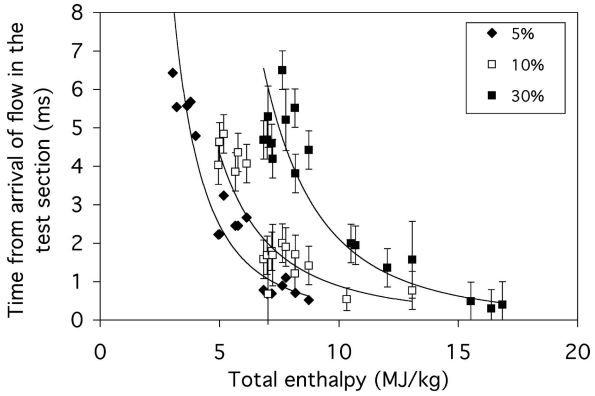

Fig. 11 Arrival time after start of flow in test section for 5, 10 and 30% contamination

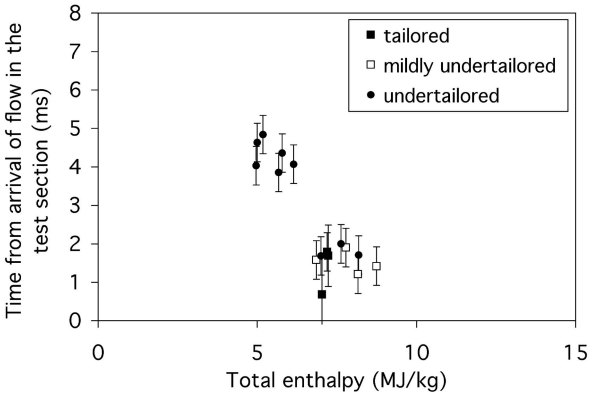

Fig. 13 Arrival time after start of flow in test section for 10% contamination—comparison for degree of tailoring

of the mean behaviour of the contamination is obtained. Different levels of contamination are presented for the following reasons. Firstly, the chosen digital oscilloscope settings limited data acquisition to 6 ms, and within this time period, significant driver gas contamination at low enthalpies was not observed to occur. Secondly, because of a combination of the hypersonic nozzle startup time, the time required for sufficient mass spectra intensity to develop in the mass spectrometer, and the effect of averaging spectra in groups of 5, typically no results are available for times earlier than approximately 500 μs after primary shock arrival in the nozzle reservoir. This means that for the higher enthalpies, significant levels of contamination are already present before sensible measurements can be made. Thus, in the figure, the 5% results range from 3 to 9 MJ/kg while the 30% results range from 7 to 17 MJ/kg. The error bars drawn represent confidence intervals for the fitting of the curves to the experimental data for each run.

Despite the use of curve fitting, the results show a reasonable amount of scatter for each contamination level. To probe possible reasons for this scatter, Figs. 12 and 13 are presented, in which the 10% contamination level results (which show the greatest degree of scatter) are subgrouped according to the main diaphragm burst pressure (28, 42, 56 and 70 MPa) and to the degree of tailoring, respectively. The results show no discernible correlation of the driver gas contamination times with the tunnel operating pressure, and similarly no discernible correlation of the driver gas contamination times with the degree of tailoring. However, the variation in the degree of tailoring was small, and in particular none of the experimental results are for overtailored operation.

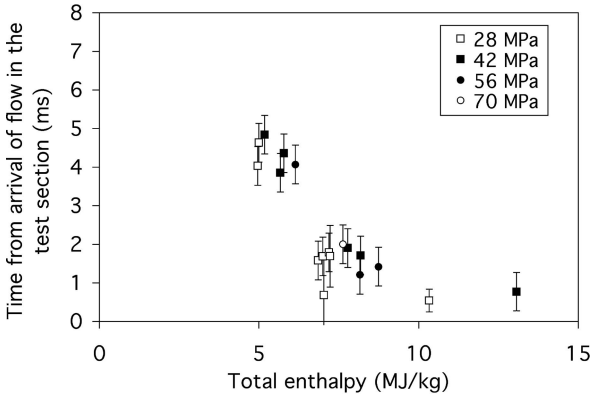

Fig. 12 Arrival time after start of flow in test section for 10% contamination—comparison for different primary diaphragm pressures

Thus, the scatter is an indication that the contamination process produces not only temporal fluctuations within each tunnel run, but also fluctuations from run to run. Nevertheless, systematic trends are evident in the results. In Fig. 11, this has been highlighted by providing power law curve fits to each contamination level group (and also by omitting the error bars for the 5% levels). The basic result is of course that the contamination occurs earlier for higher total enthalpies, in agreement with previous research. Significant contamination-free test time is to be expected at low total enthalpy, but by 9–10 MJ/kg, measurable levels of driver gas are appearing within the first millisecond after the start of flow in the test section.

Figure 14 compares the present 7.5% contamination time data with that of [7]. There is good agreement with [7] in the range 5–7 MJ/kg, while at higher enthalpies the present results predict less available test time than do those of [7]. The trends are the same however, and given the scatter in each set of results, the discrepancy is not large.

Similarly, Fig. 15 compares the present 10% contamination time data with that of [2]. The agreement is good. Also provided on Fig. 15 is a power law curve fit to the combination of 10% contamination level results from [2] (but neglecting the two zero values) and the present work. The equation for that curve is also given in the figure, complete with uncertainty values. These values were determined by normalising the experimental data by the curve fit and then computing the standard deviation of the normalised values from their mean. The two short-dashed curves in the figure graphically depict the uncertainty range of the curve fit.

Importantly, when the present results are combined with those of [2, 7], driver gas arrival time measurements using a

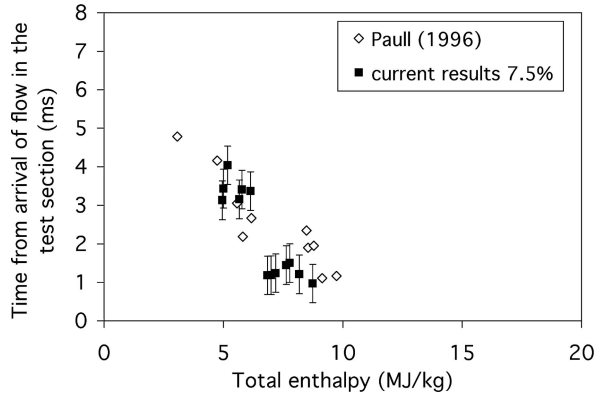

Fig. 14 Comparison of the present 7.5% contamination data with previous measurements [7]

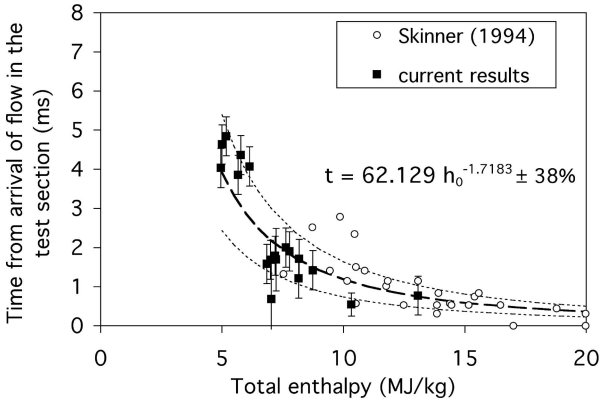

Fig. 15 Comparison of the present 10% contamination data with previous measurements [2]

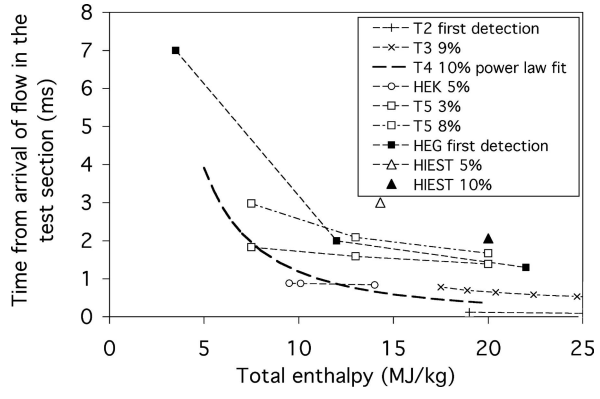

Fig. 16 Comparison between various piston-driven reflected shock tunnels

mass spectrometer now cover the entire total enthalpy range 3–20 MJ/kg, and are in agreement with measurements made using a fundamentally different technique over the range 3–9.5 MJ/kg.

Finally, Fig. 16 compares the present 10% contamination level results (in the form of the power law curve fit to the combined present and previous mass spectrometric results) to contamination time measurements from the literature for the other main piston-driven reflected shock tunnels. The results for the T2 shock tunnel at the Australian National University were measured with a quadrupole mass spectrometer, and represent the time at which driver gas is first detected in the freestream [5]. The results for T3 (also at the Australian National University, and also using a quadrupole mass spectrometer) represent the time for 9% contamination levels (adjusted from the results of [12], who quote arrival time with respect to the primary shock reflection in the shock tube. The adjustment has been made on the basis of the nozzle flow transit time measurement variation with enthalpy of the present work, which employed a similar sized nozzle to [12]). The results for the HEK and HIEST shock tunnels at JAXA in Japan, and the results for the T5 shock tunnel at CalTech in USA, were all obtained using a wedge/choked duct combination [13]. Finally, the results for the HEG shock tunnel at DLR in Germany were obtained from observations of the relative temporal behaviour of the local pitot and static pressures measured in the freestream. These results represent the time at which driver gas is first detected in the freestream [14, 15]. It is important to note that devices now exist that attempt to delay the onset of test flow contamination (see for example [14]). None of the results presented in Fig. 16 utilise such devices.

The tunnels are listed in the legend in approximate order of size, from the very small T2 to the very large HIEST. Each tunnel shows the same qualitative trends, but in general the larger the tunnel the longer the period of time available before contamination occurs. This is due to the fact that for a given enthalpy or shock speed, larger tunnels have larger test gas slug sizes in the nozzle reservoir. These results have been deliberately presented here making no attempt to scale them according to the size of the tunnel, thus enabling direct comparison of the capabilities of various piston-driven tunnels around the world.

It is worth noting that the trend with tunnel size is only a generalisation. For example, T4's contamination behaviour compared with T3 and T5, at 20 MJ/kg where data for all three tunnels can be directly compared, is not in accordance with the relevant scales of those tunnels. T3 and T4 share the same shock tube diameter (but T4's shock tube is longer) and T4 and T5 share the same shock tube length to diameter ratio (but T5's actual dimensions are 20% larger). Yet T4 has contamination times that are much less than for both T3 and T5 at that enthalpy. The reason for this is not yet understood.

5 Conclusions

A time-of-flight mass spectrometer, previously used by [2], has been improved and used to measure driver gas contamination levels in the test section of the T4 shock tunnel, as a function of time after the onset of flow in the test section, and over the total enthalpy range 3–17 MJ/kg. Arrival times for various contamination levels have been extracted

from these measurements. The results are, to within the scatter in the data, independent of the tunnel operating pressure and independent of the degree of tailoring (which was either tailored or undertailored). The scatter indicates that while the early contamination of the air test slug in the shock tube is broadly a function of the total enthalpy, there are inherent fluctuations associated with the mechanism responsible for the early contamination, both within a given run and from run to run. The results confirm measurements made by [7] using a choked duct driver gas detector at these conditions, and extend the range of previous mass spectrometer measurements for T4 [2] to that of 3–20 MJ/kg. A comparison of the contamination behaviour of various piston-driven reflected shock tunnels has been made.

Acknowledgements This work was financially assisted by the Australian Research Council and the Japanese Science and Technology Corporation. The authors gratefully acknowledge fruitful discussions with Prof Allan Paull; the technical expertise of George Dick, Ken Dudson and Joe Gisa; and the operation of T4 by Chris Goyne, Mark Kendall, Robert Palmer, Adrian Smith and Mark Sutcliffe.

References

1. Stalker, R.J.: Development of a hypervelocity wind tunnel. Aeronautical J. **76**, 374–384 (1972)
2. Skinner, K.A.: Mass spectrometry in shock tunnel experiments of hypersonic combustion. PhD Thesis, The University of Queensland (1994)
3. Davies, L., Wilson, J.L.: Influence of reflected shock and boundary–layer interaction on shock-tube flows. Shock tube symposium, Phys. Fluids Suppl. **1**, I37–I43 (1969)
4. Stalker, R.J., Crane, K.C.A.: Driver gas contamination in a high enthalpy reflected shock tunnel. AIAA J. **16**, 277–278 (1978)
5. Slade, J.C., Crane, K.C., Stalker, R.J.: Driver gas detection by quadrupole mass spectrometry in shock tunnels, Vol. 1, pp. 293–298. Shock Waves @ Marseille, Springer-Verlag (1995)
6. Sudani, N., Valiferdowsi, B., Hornung, H.G.: Test time increase by delaying driver gas contamination for reflected shock tunnels. AIAA J. **38**(9), 1497–1503 (2000)
7. Paull, A.: A simple shock tunnel driver gas detector. Shock Waves **6**(5), 309–312 (1996)
8. Chue, R.S.M., Eitelberg, G.: Studies of the transient flows in high enthalpy shock tunnels. Exp. Fluids **25**, 474–486 (1998)
9. Burtschell, Y., Cardoso, M., Zeitoun, D.E.: Numerical analysis of reducing driver gas contamination in impulse shock tunnels. AIAA J. **39**(12), 2357–2365 (2001)
10. Goozee, R.: Simulation of a complete shock tunnel with parallel computer codes. PhD Dissertation, The University of Queensland, Brisbane, Australia (2003)
11. Boyce, R.R., Takahashi, M., Stalker, R.J.: Mass spectrometric measurements of the freestream composition in the T4 free-piston shock-tunnel. Shock Waves J. (in press). DOI 10.1007/s00193-005-0275-4 (2005)
12. Crane, K.C.A., Stalker, R.J.: Mass-spectrometric analysis of hypersonic flows. J. Phys. D: Appl. Phys. **10**, 679–695 (1977)
13. Sato, K., Komuro, T., Sato, M., Sudani, N., Itoh, K.: Detection of driver gas contamination in high-enthalpy shock tunnels. Jpn. Soc. Aeronaut. Space Sci. J. **47**(551) 470–473 (1999)
14. Hannemann, K., Schnieder, M., Reimann, B., Martinez Schramm, J.: The influence and the delay of driver gas contamination in HEG. AIAA-2000-2593, Proc. 21st AIAA Aerodynamic Measurement Technology and Ground Testing Conference, Denver (2000)
15. Gardner, A.D.: HyShot scramjet testing in the HEG. PhD Dissertation, The University of Queensland, Brisbane, Australia (2005)